

Multi-State Non-Adiabatic Direct-Dynamics on Propagated Diabatic Potential Energy Surfaces

Gareth W. Richings¹, Graham A. Worth^{2,*}

School of Chemistry, University of Birmingham, Edgbaston, Birmingham, B15 2TT, UK

Abstract

An extension of a recent diabatisation scheme for use in direct-dynamics variational multi-configuration Gaussian (DD-vMCG) quantum dynamics calculations is presented which allows the treatment of systems with more than two electronic states. Methodological updates to the DD-vMCG implementation are presented along with applications of the method to 2-, 3- and 4-state models of the butatriene cation. As a demonstration of the utility of the method, results of 3-state, full-dimensional calculations on the DNA base, thymine, are included, showing the energy dissipation through wavefunction population transfer between states.

Keywords: Direct-dynamics, Diabatisation, vMCG, Thymine

2010 MSC: 00-01, 99-00

1. Introduction

The methods of quantum nuclear dynamics are important in the study of energy dissipation in molecular systems of interest in chemistry and biology. Over the past decade they have shown particular utility in studying photo-excited molecular dynamics and unravelling the results of pulsed laser femtochemistry experiments. Recent examples of joint experimental and quantum dynamics studies from our group include the photochemistry of benzene [1] and pyrrole [2]. The use of such methods by the non-specialist has, however been restricted historically with the main stumbling block being the construction of the potential energy surfaces (PESs) over which the nuclear wavepacket moves. In order to overcome this difficulty

much recent work has focused on the development of direct-dynamics (DD) methods where the PESs are constructed concurrent with the dynamics[3, 4]. Methods such as trajectory surface hopping[5, 6, 7] and *ab initio* multiple spawning[8, 9, 10] have proved their usefulness in many studies. Surface hopping, however, is a semi-classical method and in spawning the basis functions follow classical trajectories which means quantum effects may be hard to describe accurately. The inclusion of quantum mechanical effects in the basis functions can be achieved by use of the variational multi-configuration Gaussian (vMCG) method and its DD variant, DD-vMCG[11, 12, 13, 14, 15, 16, 17, 18, 19, 20].

After photo-excitation, energy dissipation can occur through transfer of wavepacket density

*Corresponding author

Email address: g.a.worth@uc1.ac.uk (Graham A. Worth)

¹Current address: Department of Chemistry, University of Warwick, Coventry, CV4 7AL

²Current address: Department of Chemistry, University College London, Gordon Street, London, WC1H 0AJ

35 between electronic states in what are termed
 non-adiabatic processes. This means that cou-
 40 pled multiple PESs must be included in cal-
 culations studying these processes. The DD-
 vMCG method requires the use of smooth dia-
 batic PESs on which the wavepacket evolves i.e.
 the PESs are generated by transforming the sur-
 faces produced by electronic structure methods
 to remove the infinite couplings between them at
 points of degeneracy. Originally DD-vMCG used
 45 a variant of Köppel’s regularisation diabatisation
 method[21, 22, 23] to obtain such PESs, but this
 method is restricted to two electronic states and
 systems that cross states around a well-defined
 point. Recently,[24] we introduced the *propaga-*
 50 *tion diabatisation* method which allows construc-
 tion of global diabatic states on-the-fly by propa-
 gation of the adiabatic/diabatic transformation
 matrix along paths in molecular configuration
 space. That work demonstrated the method on a
 55 two-state model, however, it was noted that the
 method could be extended to treat any number
 of states. Herein we present the first DD-vMCG
 calculations performed using this scheme on more
 than two states.

60 We first consider the butatriene cation, as
 tested in our earlier work[24], using three and
 four states. Butatriene is an ideal test of diabati-
 sation schemes because of its well characterised
 conical intersection (CI) between the ground and
 65 first-excited states[11, 25]. We return to it as the
 previous calculations indicated the presence of a
 higher lying state that becomes degenerate with
 the first-excited state at geometries away from
 the intersection, but accessible. We now confirm
 70 the presence of this additional crossing.

The final part of this work is a brief study of
 thymine. The use of quantum dynamics to study
 DNA bases is of great interest as it is thought that

non-adiabatic effects are responsible for the rapid
 75 dissipation of energy after absorption of ultra-
 violet photons. This process has been studied in-
 tensely, both theoretically[9, 19, 26, 27, 28, 29]
 and experimentally[30, 31, 32] (for recent re-
 views see [33, 34, 35]), with the actual path-
 80 ways debated. It is thought that the three
 lowest lying electronic states are responsible for
 the dissipation, which occurs over three distinct
 timescales[33]. Thymine has been studied using
 DD-vMCG before with only the two upper states
 85 included and in reduced dimensionality[19]. Our
 calculations here include all modes and three
 states and show wavepacket transfer between
 them, an important step towards being able to
 fully describe this process.

90 2. Methodology

The DD-vMCG method was recently re-
 viewed elsewhere[12], but briefly, the nuclear
 wavefunction is expanded as a linear combi-
 nation of time-dependent Gaussian wavepackets
 (GWPs),

$$\Psi(\mathbf{r}, t) = \sum_{j=1}^N A_j(t) g_j(\mathbf{r}, t) \quad (1)$$

Applying the Dirac-Frenkel variational principle
 yields equations-of-motion for the vector of coef-
 ficients, A_j , and for the GWPs, g_j , respectively

$$\dot{\mathbf{A}} = i\mathbf{S}^{-1}(\mathbf{H} - i\boldsymbol{\tau})\mathbf{A} \quad (2a)$$

$$i\mathbf{C}\dot{\mathbf{A}} = \mathbf{Y} \quad (2b)$$

where \mathbf{S} is the GWP overlap matrix, \mathbf{H} the
 95 GWP Hamiltonian matrix, $\boldsymbol{\tau}$ the matrix of over-
 lap time-derivatives, $\langle g_i | \dot{g}_j \rangle$, and $\dot{\mathbf{A}}$ the vector of
 time-derivatives of the parameters defining the
 individual GWPs.

The \mathbf{C} -matrix and \mathbf{Y} -vector involve a projector out of the space of the GWPs,

$$\hat{P} = \sum_{ij} |g_i\rangle S_{ij}^{-1} \langle g_j| \quad . \quad (3)$$

The use of a projector involving non-orthogonal functions, however, can cause numerical problems due to the inverse of the overlap matrix becoming singular when the functions become linearly dependent. We have thus implemented a modified version of these equations, whereby Gram-Schmidt orthonormalisation is used to generate an orthonormal basis, $\{\phi_i\}$, and a GWP found to be linearly dependent to those preceding it, has zero-coefficient in this matrix. This allows the construction of a projector which does not involve the inverse of the overlap matrix

$$C_{j\alpha, l\beta} = \rho_{jl} \left\langle \frac{\partial g_j}{\partial \lambda_{j\alpha}} \middle| 1 - \sum_r |\phi_r\rangle \langle \phi_r| \middle| \frac{\partial g_l}{\partial \lambda_{l\beta}} \right\rangle \quad (4a)$$

$$Y_{j\alpha} = \sum_l \rho_{jl} \left\langle \frac{\partial g_j}{\partial \lambda_{j\alpha}} \middle| \left(1 - \sum_r |\phi_r\rangle \langle \phi_r| \right) \hat{H} \middle| g_l \right\rangle \quad (4b)$$

For non-adiabatic systems with multiple potential energy surfaces the equations are extended by either using different sets of GWPs for each state (multi-set formalism), or a single set of GWPs with vectors to index the expansion coefficients for the states (single-set formalism). For details see Ref. [36].

The on-the-fly diabatisation uses the propagation of the adiabatic/diabatic transformation matrix, \mathbf{K} . Defining the non-adiabatic coupling term (NACTs) between adiabatic states ψ_i and ψ_j ,

$$\mathbf{F}_{\alpha, ij} = \frac{\langle \psi_i | \nabla_{\alpha} \hat{H} | \psi_j \rangle}{V_{jj} - V_{ii}} \quad (5)$$

where V_{ii} and V_{jj} are their respective energies. In this work ∇_{α} implies differentiation with respect to the nuclear coordinate, R_{α} . The diabatisation

method uses the relationship[37]

$$\nabla \mathbf{K} \approx -\mathbf{F} \mathbf{K} \quad (6)$$

where \mathbf{F} is the matrix of NACT vectors. This expression is exact if the basis set of electronic states ψ_j is complete, with the curl of the couplings being zero[37], but is necessarily approximate in practical calculations due to truncation of the electronic basis. However, near CIs, the regions where accuracy of the diabatisation procedure is most important, the non-removable couplings (to the excluded states) are insignificant[38] and the expression valid.

Integration of this expression along some path between two molecular geometries, \mathbf{R} and $\mathbf{R} + \Delta \mathbf{R}$, yields the transformation matrix at the end point[24, 39].

$$\mathbf{K}(\mathbf{R} + \Delta \mathbf{R}) = \exp \left(- \int_{\mathbf{R}}^{\mathbf{R} + \Delta \mathbf{R}} \mathbf{F} \cdot d\mathbf{R} \right) \mathbf{K}(\mathbf{R}) \quad (7)$$

This scheme can be applied to any number of electronic states if the NACTs between all pairs of states are calculated. Inclusion of extra states alleviates problems with the inaccuracy of Eq. (6)[40], particularly that integration around a closed path does not bring the transformation matrix back to where it started[41]. The multi-state method has now been implemented using NACTs calculated using Molpro 15[42]. The algorithm has been modified slightly to improve its stability: it now uses a linear, rather than Shepard, interpolation of the numerator of Eq. (5) when performing the numerical integration in Eq. (7). In the original implementation extra *ab initio* points would be calculated along the path over which the integral was evaluated if the path length was greater than the distance parameter used to determine when a new potential energy should be calculated (a new point is

135 calculated if the centre of a Gaussian function ex-
ceeds that distance from the nearest geometry in
the database). This is an unnecessary complica-
tion and is hence no longer done, so the integral

140 In the following we apply this method, imple-
mented in a development version of the Quantics
package[43], to two molecules with more than two
electronic states.

3. Results

145 3.1. Butatriene

We return to the butatriene cation to demon-
strate the capabilities of the extended propaga-
tion diabatisation method. In Ref. [24] it was
noted that a high lying intruder state was sus-
150 pected during the course of the dynamics, due
to the NACTs at adjacent database points be-
ing orthogonal. A more complete description of
the manifold of states is thus necessary to get a
complete picture of the dynamics, and here we
155 present results of calculations performed using
2, 3 and 4 states, along two ground state nor-
mal modes representing the nuclear degrees of
freedoms. These are the $5A_u$ (molecular torsion
mode) and $14A_g$ (symmetric stretch of the mid-
160 dle C-C bond) modes. The 2-state model has
been recalculated here using the improved for-
mulation of the dynamics and diabatisation and
with Molpro 15 to compare to the 3- and 4-state
simulations.

165 The electronic structure calculations were
performed using the complete active space self-
consistent field method (CASSCF) with state av-
eraging (SA) (the weighting of each state be-
ing equal) and 5 electrons in 6 orbitals (cov-
170 ering the π -system) with the 3-21G basis set.
The normal modes were calculated at the neu-

tral ground-state minimum energy geometry us-
ing CASSCF(6,6) and the same basis set and
mass-frequency scaled to provide unitless coor-
175 dinates in the dynamics. 25 GWPs per state
were used in the nuclear wavefunction expansion
(the multi-set formulation), initially evenly dis-
tributed around the centre of the wavefunction
placed at the Franck-Condon (FC) point on the
180 first excited state. The GWPs had frozen widths
of $1/\sqrt{2}$ along both degrees of freedom, which
in the mass-frequency scaled coordinate system
represents the neutral vibrational ground-state
wavefunction. PES database points were cal-
185 culated at the centres of these initial positions,
and extra points were calculated as GWPs moved
more than 0.25 au from the position of the near-
est database geometry. The dynamics were run
for 100 fs with data output every 0.5 fs using a
190 fifth-order Runge-Kutta integrator with accuracy
cutoff of 10^{-6} to solve the equations-of-motion of
both the GWPs and the \mathbf{A} -vector. Symmetry
of the wavefunction was enforced by pairing the
equivalent GWPs and their coefficients as out-
195 lined before[24].

In figures 1 (a) and (b), we see the adiabatic
and diabatic surfaces, respectively, resulting from
the 2-state calculation, the former clearly show-
ing the well known CI at about 2 units along the
 $14A_g$ mode and a planar geometry (a value of 0
in the $5A_u$ mode). The latter figure shows the
smooth crossing of the diabatic surfaces (labelled
 \tilde{X} and \tilde{A} in increasing energy order at the FC
point) around the CI that we would expect from a
successful diabatisation scheme, and corresponds
205 to the result from our previous work.

Moving on to figures 1 (c) and (d), we show
the adiabatic and diabatic surfaces, respectively,
resulting from a calculation using 3 states. The
CI between the D_0 and D_1 adiabatic states is
210

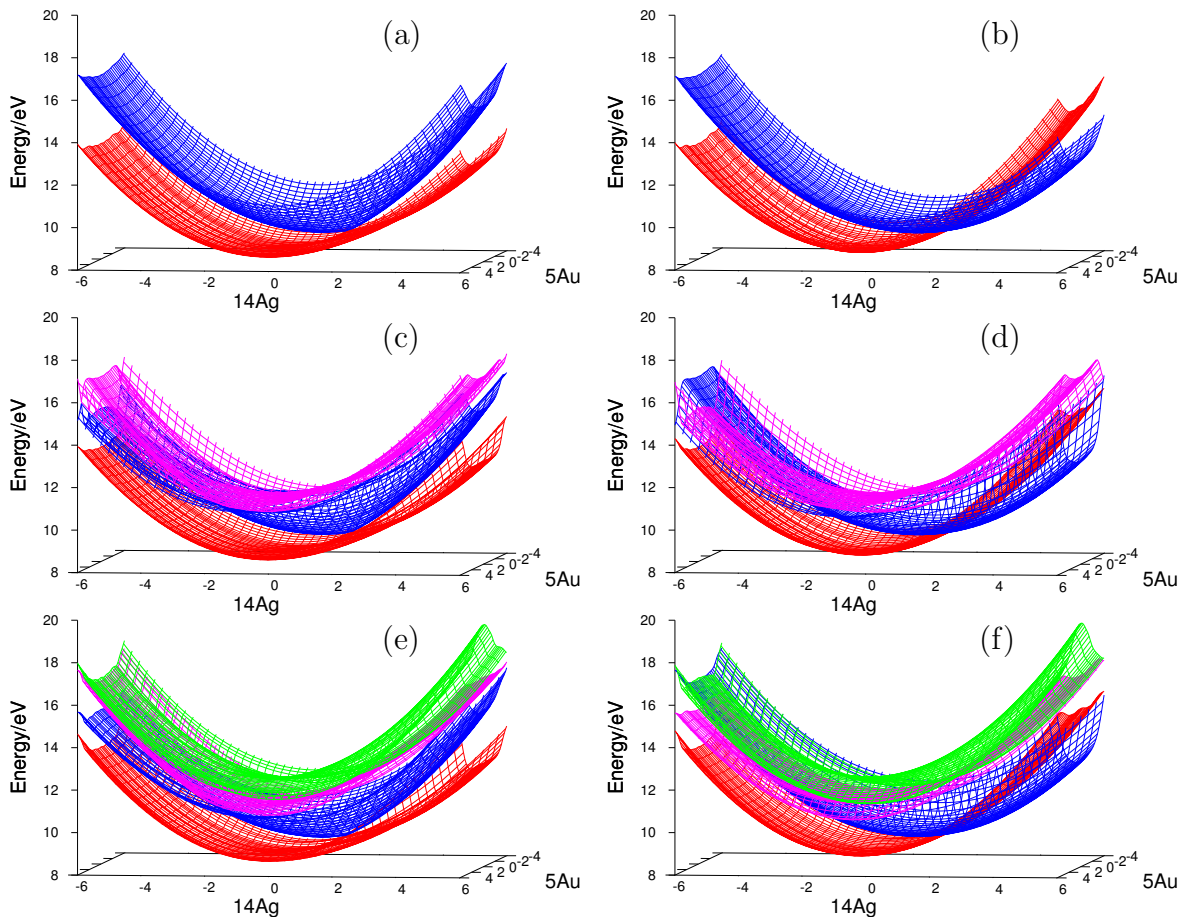


Figure 1: Potential energy surfaces of the butatriene cation calculated at the SA-CASSCF(5,6)/3-21G level using Molpro 15 during DD-vMCG simulations as outlined in the text. (a) Adiabatic surfaces for the 2-state model. (b) Diabatic surfaces for the 2-state model. (c) Adiabatic surfaces for the 3-state model. (d) Diabatic surfaces for the 3-state model. (e) Adiabatic surfaces for the 4-state model. (f) Diabatic surfaces for the 4-state model. For the adiabatic plots, the red surface is the D_0 state, the blue is D_1 , the pink is D_2 and the green surface is D_3 . For the diabatic plots, the red surface is the \tilde{X} state, the blue is \tilde{A} , the pink is diabat \tilde{B} and the green surface is state \tilde{C} .

found at the same position as in the 2-state calculation. At this point the D_2 state is significantly higher in energy than the other two states, hence its coupling to them is relatively weak, meaning that the shapes of the lower two surfaces are relatively unaffected by the inclusion of the third state. The major difference from the 2-state calculation occurs at about -2 in the $14A_g$ coordinate where there is an intersection between the D_0 and D_1 adiabatic states (see figure 1(c)). At larger magnitude values of the $5A_u$ coordinate those two states also come close in energy and form seams of intersection. In figure 1(d), the di-

225 abatic states \tilde{A} and \tilde{B} cross at these positions in configuration space. Because of these latter intersections, at large negative values of the $14A_g$ coordinate the D_1 state (corresponding to the \tilde{B} diabat here) has negative curvature in the $5A_u$ coordinate close to planar geometries; a feature not seen in the 2-state calculation.

The negative curvature is also seen in the D_1 adiabatic surface in the 4-state calculation (figure 1(e)), but is now present on the higher energy \tilde{C} diabat instead of on the \tilde{B} (figure 1(f)). Indeed this curvature is a feature of the \tilde{C} diabat at all values of the $14A_g$ coordinate, includ-

ing at positive values where it corresponds to the D_3 adiabatic state. It is also this diabatic state which drops in energy towards the two lowest energy states at large values of the $5A_u$ coordinate rather than the \tilde{B} state in the 3-state calculation.

We should note that the shape of the \tilde{X} and \tilde{A} states are fairly consistent for each of the three calculations in the lower energy regions where the wavepacket is likely to be moving, it having started at the FC point on the \tilde{A} state. Also noteworthy is that the \tilde{B} and \tilde{C} states are relatively high in energy (except for the latter at geometries far from planar), so we would not expect either to be greatly populated during the course of the dynamics.

In Figure 2 we present the populations of the \tilde{A} diabatic state (that corresponding to D_1 at the FC point) as a function of propagation time, using 2, 3 and 4 states in the calculations.

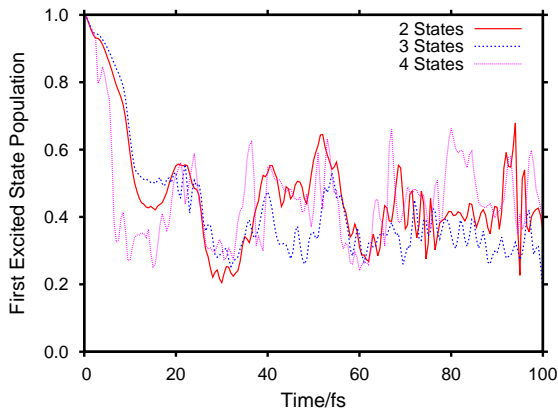


Figure 2: Wavepacket population of the first-excited, diabatic, cation (\tilde{A}) state of butatriene as a function of propagation time using a two-dimensional model consisting of the $5A_u$ and $14A_g$ normal modes and the DD-vMCG method with SA-CASSCF(5,6)/3-21G calculated potential energy surfaces. Red, solid line corresponds to propagation on 2 surfaces. Blue, dashed line corresponds to propagation on 3 surfaces. Pink, dotted line corresponds to propagation on 4 surfaces.

The first feature to note from the figure is the initial similarity of the plots for the 2- and 3-state calculations; there is an immediate, rapid

depopulation of the \tilde{A} state down to around 0.5 after 15 fs as the CI between the D_0 and D_1 states is encountered by the wavepacket. The population of the \tilde{A} state briefly stays fairly constant in the 3-state calculation whilst the state is partially repopulated in the 2-state calculation as the wavepacket moves back past the CI. In both cases the population then drops to just above 0.2 after about 30 fs as there is another pass of the CI before the state is again partially repopulated to just over 0.5 in the 2-state case and just over 0.4 in the 3-state case. There is a depopulation respectively to 0.4 and just over 0.2 respectively between 40 and 50 fs before a final cycle over the next 15 fs or so before the population settles down to a less structured oscillation from 70 fs onwards as the wavepacket evolves away from its oscillation close to the CI.

Turning now to the 4-state calculation; the plot of the population of the \tilde{A} state differs from that in the other calculations almost from the start. The initial population decrease is much more rapid, including a very brief repopulation after about 5 fs, reaching a level of 0.3, before repopulation to about 0.5 after 20 fs. This is followed by a depopulation and repopulation cycle to the same levels over the next 20 fs. The population then briefly drops before recovering and then drops to just over 0.2 for 10 fs around the 60 fs mark. A less structured pattern of population transfer then takes over for the rest of the propagation.

With regards to the higher energy states in the 3- and 4-state calculations, we will deal with the populations of the states when using the 4-state model first as plotted in Figure 3(a). The population of the \tilde{B} state is 0 until 6.5 fs, before briefly rising to a maximum of 2.4×10^{-2} at 15.5 fs. Subsequent to this the population oscil-

lates but stays below 3×10^{-3} until the end of
the propagation. The population of the \tilde{C} state
is even lower, being 0 until 6.5 fs and reaching a
maximum of 4×10^{-4} during the course of the
propagation. Thus there is some very small pop-
ulation transfer to these states during the course
of the dynamics when using the 4-state model.

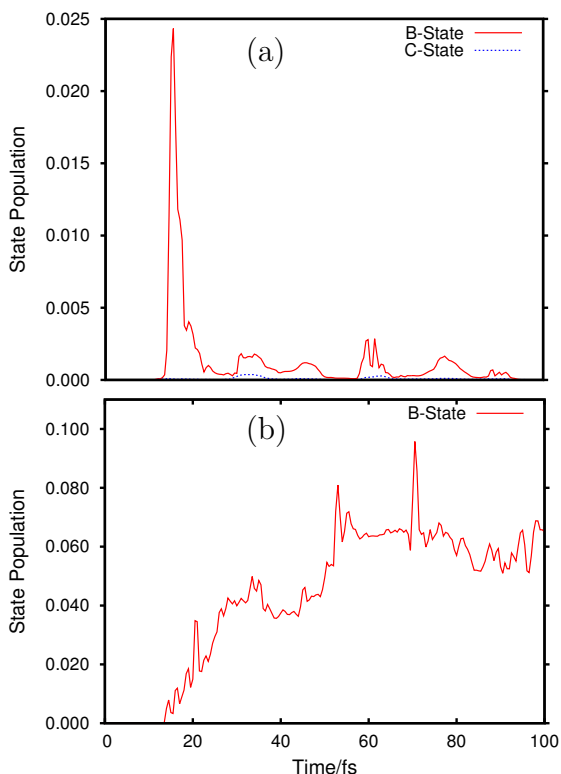


Figure 3: Wavepacket population of the higher-excited, diabatic, cation states of butatriene as a function of propagation time using (a) a four-state model and (b) a three-state model.

The population transfer to the \tilde{B} state is more significant when using the 3-state model and a plot is shown in Figure 3(b). The population is 0 until 13.5 fs, before rising to a plateau at around 0.04 after 28 fs. The population then steps up again to around 0.06 after 50 fs; this level is maintained, apart from brief spikes up to 0.08 and 0.1, until 80 fs when there is a slight drop in the population before recovery at the end of the propa-

gation.

The earlier rise in the population coincides with the period of stable population of the \tilde{A} state seen in Figure 2, indicating that it is the motion of the wavepacket in the negative $14A_g$ direction, back past the D_0/D_1 CI then on towards the crossing between the two excited states that is responsible for both sets of features. The later rise also corresponds to the increase in \tilde{A} state population seen at the same time. That there is no decrease in the population accompanying similar changes in the \tilde{A} state suggests that that component of the wavefunction is trapped on the higher energy state.

The relatively low population of the higher excited states in the 4-state calculation is indicative of a higher energy crossing between the \tilde{A} and \tilde{B} states, the result of the inclusion of the fourth state. The numbers involved in both calculations are small though and do not explain the change, between the 3- and 4-state calculations, in the behaviour of the \tilde{A} state population seen in Figure 2. To give further insight into this change the width of the wavepacket, defined as $\langle dq \rangle = \sqrt{\langle q^2 \rangle - \langle q \rangle^2}$, along the $5A_u$ mode on the \tilde{X} state is shown in Figure 4. Immediately apparent is the close similarity between the 2- and 3-state plots, particularly over the first 80 fs, which mirrors the comparable population changes seen in Figure 2, whilst the width of the wavepacket in the 4-state calculation is noticeably different from the start. The wavepacket initially spreads in the latter case rather than contracts, and then follows a more rapidly oscillatory pattern as the propagation progresses. From this it is clear that, despite the apparent similarities in the PESs of the \tilde{X} and \tilde{A} states as shown in Figure 1, the PESs in the 4-state calculation are sufficiently distinct to give different dynamics, which results in the

changes in the population plots seen in Figure 2

355 when a fourth state is added.

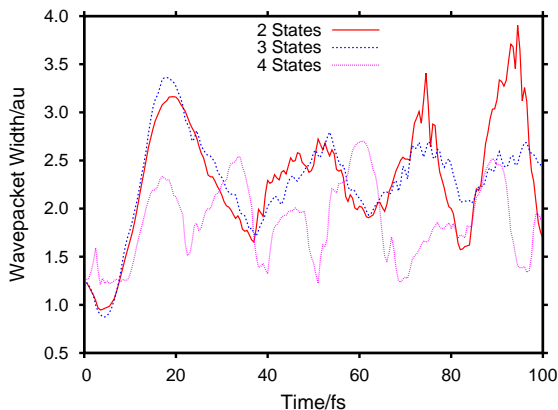


Figure 4: Width of the wavepacket on the ground, diabatic, cation (\tilde{X}) state of butatriene along the $5A_u$ mode as a function of propagation time. Red, solid line corresponds to propagation on 2 surfaces. Blue, dashed line corresponds to propagation on 3 surfaces. Pink, dotted line corresponds to propagation on 4 surfaces.

From these results it is apparent that inclusion of more states in a quantum dynamics calculation affects the results even if the propagated wavepacket only populates those states to a small extent. The changing behaviour of the dynamics is driven by the differing shape of the PESs caused by the inclusion of more states.

3.2. Thymine

365 Having shown the difference in the dynamics caused by the inclusion of more electronic states in a reduced dimensionality model of a small molecular system, we now consider a larger molecule, the photophysics of which are of broad interest, namely thymine.

A previous work by one of us and others involved performing DD-vMCG calculations on the first two excited states of thymine, S_1 and S_2 , the former of (n, π^*) character, the latter with (π, π^*) character[19]. That work was limited to these two states by the use of the regularisation diabatisation scheme, and to a maximum of 8 pairs

of GWPs (1 GWP per state for each pair). As the interest in thymine and other DNA/RNA bases from a photophysics point of view is in the mechanism of deactivation to the ground state of the molecule on excitation with UV light, it is important to include the full manifold of states which are important in the dynamics: the bright state to which the molecule is excited, the final ground state and any intermediate states *via* which deactivation can occur. With the implementation of the propagation diabatisation scheme we are in a position to return to thymine and include the three states of interest, fully diabatised, in the dynamics calculation. In addition, with increased computer power and an OpenMP parallelised version of the Quantics code we can use a far greater number of GWPs in the wavefunction.

390 As in earlier papers[19, 26] we used the CASSCF(8,6)/6-31G* level of theory for the electronic structure calculations. The active space consisted of the three highest energy π -orbitals, that containing the lone pair on O_8 and the two lowest energy, unoccupied, π^* -orbitals. After optimisation of thymine's ground state geometry at this level and calculation of the 39 normal modes at that point, a 1 GWP, DD-vMCG relaxation calculation was performed on the PES generated at the SA-CASSCF(8,6)/6-31G* level in order to give an improved approximation of the FC point. The wavepacket was vertically excited from this geometry to the second excited state, (π, π^*) , and allowed to propagate for 80 fs.

405 The same procedure was followed for the propagation of the thymine wavepacket as was used for butatriene in terms of the integrator and the GWP widths. The first difference from butatriene came in the number of GWPs used. Two calculations were performed, one with 40 GWPs and one with 79 (i.e. one GWP at the centre of

the initial wavepacket and one or two respectively along each normal mode), in the single-set formalism i.e. with the same set of GWPs used to expand the wavefunction on all three states (resulting in reduced computational effort and increased numerical stability). The 40 GWP calculation was started with a database populated by 79 electronic structure points, located at the geometries initially occupied in the 79 GWP calculation (the 40 GWPs' geometries coincide with 40 of those points, the remaining 39 are symmetrically positioned along the modes to the other side of the central GWP). The calculations also differed from those on butatriene in the frequency of updating the electronic structure database; in this case a distance between the GWP centres from the nearest database point of greater than 0.1 au of was used to trigger a new energy calculation. In addition, no symmetry of the wavepacket was enforced during these calculations, as doing so was found to cause the annihilation of the wavepacket on surfaces where more than one node was present (unfeasibly more GWPs would need to be included to avoid this and to enforce symmetry).

In figure 5(a) we present results from the calculation on thymine with 40 GWPs, where we show the populations of the three diabatic states included: at the FC point \tilde{X} corresponds to S_0 , \tilde{A} to the (n, π^*) , S_1 state and \tilde{B} to the (π, π^*) , S_2 state. This calculation generated a total of 241 database points (i.e. an additional 162 over the initial set) and required over 233 hours of CPU time to propagate the wavepacket (in addition to the time needed for the electronic structure calculations).

From the plot it can be seen that depopulation of the \tilde{B} state begins immediately after excitation, but what is less clear is that population

transfers to both the \tilde{X} and \tilde{A} states. The population of the \tilde{X} state rises over the first 5 fs but then levels off for the next 20 fs in the 0.01-0.03 range, before increasing again to just below 0.2 at around 60 fs, then slightly decreasing to the end. The population of the \tilde{B} state more or less mirrors that of the \tilde{X} . There is slow population transfer to the \tilde{A} state, rising to about 0.01 after 30 fs before staying close to that mark for the next 30 fs. In the final 20 fs the \tilde{A} state population goes through another period of increase reaching just below 0.04 at the end. This final period matches that of the slow decrease in population of the \tilde{X} state suggesting a pathway between the two. The numerical noise in the data makes detailed description difficult but it is apparent that about 20% of the population in the initial $\tilde{B}/\pi\pi^*$ state is lost within 80 fs of excitation.

In figure 5(b) we plot the state populations using a basis of 79 GWPs i.e. initially one placed at the centre of the wavepacket and two others displaced along each normal mode, either side of and equidistant from the central point. This propagation generated a total of 372 electronic structure database points and took a total of over 2056 CPU hours (in addition to the time required for the electronic structure calculations) to complete.

The plot is less noisy than that using 40 GWPs, allowing a clearer picture of the dynamics. Similar to the smaller calculation, population transfer from the \tilde{B} state begins immediately to both lower states, with the bulk going to the \tilde{X} state. After the increase over the first 10 fs of the \tilde{X} state population, it dips slightly before starting to rise again after 25 fs. A further dip between 40 and 50 fs is followed by a steeper rise in population to the end of the propagation. These population changes are again almost mirrored by those in the \tilde{B} state. The population transfer to

495 the \tilde{A} state is smaller than that in the 40 GWP case, having a small peak between 35 and 40 fs before dropping back towards zero. The final 25 fs see the most significant population transfer to the \tilde{A} state, peaking at 0.03. Nearly 25% of the \tilde{B} wavepacket population moves to the lower diabat over the course of 80 fs, slightly more than when fewer GWPs were used.

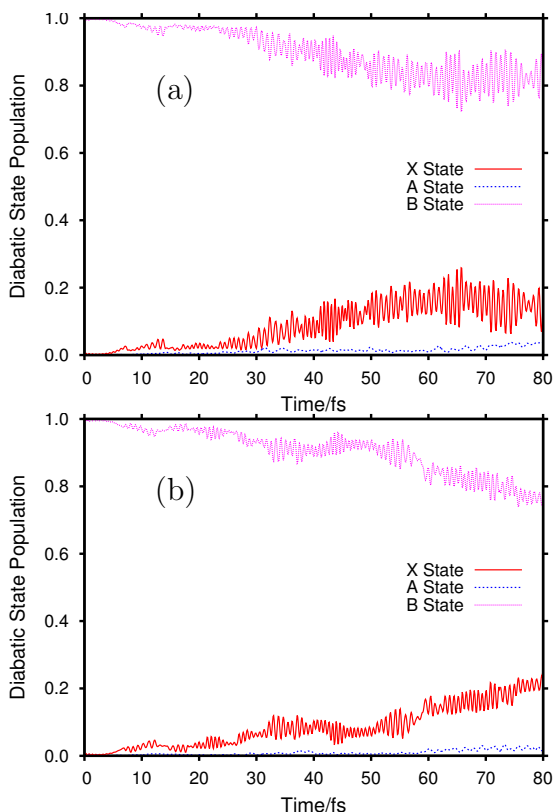


Figure 5: Wavepacket population of the diabatic states of thymine as a function of propagation time using a full-dimensional model consisting of 39 normal modes using the DD-vMCG method with (a) 40 GWPs and (b) 79 GWPs. Both used SA-CASSCF(8,6)/6-31G* to calculate the potential energy surfaces. Red, solid line corresponds to population on the \tilde{X} state. Blue, dashed line corresponds to population on the \tilde{A} state. Pink, dotted line corresponds to population on the \tilde{B} state.

The overall level of population transfer is similar to that seen in Ref. [19], however, the population transfer in that work was more rapid than here because the wavepacket was given a non-zero

initial momentum along particular modes in order to push it towards particular CIs. Here the wavepacket is initialised with zero momentum in all directions and allowed to propagate with no preference towards any particular geometry.

The general picture seen in the 40 and 79 GWP calculations is the similar but with some differences. Longer propagation times would confirm whether this pattern is continued, but improvements in the propagation algorithms and/or computational resources would be required to confirm this or otherwise

4. Conclusions

In this letter we have presented the first set of results using the DD-vMCG quantum dynamics method on more than 2 diabatic states. This has been allowed by extension of our previously published propagation diabatisation scheme and use of the Molpro package which generates couplings between all pairs of electronic states.

Results on the butatriene cation reveal the crossing of the D_1 and D_2 states as was inferred in our earlier work when only two states could be considered. We showed the importance of including higher energy states, even when the nuclear dynamics proceeds almost entirely on the lowest two states, as noticeable changes in the behaviour of the wavepacket (in terms of population transfer and wavepacket spread) result.

We have also applied the method to a full-dimensional dynamics calculation on the DNA base, thymine, including the three states thought to be involved in the dissipation of energy after absorption of a UV photon. We see population transfer beginning almost immediately after excitation, predominantly to the ground state, but also to the first excited state. Further work will be required to extract useful decay lifetimes, but

these initial results show that it is possible to model such an important system using a quantum mechanical method.

Acknowledgments

550 This work was funded by the EPSRC under grant EP/K037943/1.

References

- [1] T. J. Penfold, R. Spesyvtsev, O. Kirkby, R. S. Minns, D. Parker, H. H. F. Fielding, G. A. Worth, Quantum dynamics study of the competing ultrafast intersystem crossing and internal conversion in the “channel 3” region of benzene, *J. Chem. Phys.* 137 (2012) 204310–204312.
- 590
- [2] G. Wu, S. P. Neville, O. Schalk, T. Sekikawa, M. N. R. Ashfold, G. A. Worth, A. Stolow, Excited State Non-Adiabatic Dynamics of Pyrrole: A Time-Resolved Photoelectron Spectroscopy and Quantum Dynamics Study, *J. Chem. Phys.* 142 (2015) 074302/1–12.
- 560
- [3] M. Persico, G. Granucci, An overview of nonadiabatic dynamics simulation methods, with focus on the direct approach versus the fitting of potential energy surfaces, *Theor. Chem. Acc.* 133 (2014) 1526/1–28.
- 570
- [4] G. A. Worth, M. A. Robb, B. Lasorne, Solving the time-dependent Schrödinger Equation in one step: Direct Dynamics of Non-adiabatic Systems., *Mol. Phys.* 106 (2008) 2077–2091.
- 575
- [5] J. C. Tully, R. K. Preston, Trajectory surface hopping approach to nonadiabatic molecular collisions: The reaction of H^+ with D_2 , *J. Chem. Phys.* 55 (1971) 562–572.
- 580
- [6] J. C. Tully, Molecular dynamics with electronic transitions, *J. Chem. Phys.* 93 (1990) 1061–1071.
- [7] M. Richter, P. Marquetand, J. González-Vázquez, I. Sola, L. González, Femtosecond Intersystem Crossing in the DNA Nucleobase Cytosine, *J. Phys. Chem. Lett.* 3 (2012) 3090–3095.
- [8] M. Ben-Nun, T. J. Martínez, *Ab Initio* quantum molecular dynamics, *Adv. Chem. Phys.* 121 (2002) 439–512.
- [9] H. R. Hudock, B. G. Levine, A. L. Thompson, H. Satzger, D. Townsend, N. Gador, S. Ullrich, A. Stolow, T. J. Martínez, *Ab initio* molecular dynamics and time-resolved photoelectron spectroscopy of electronically excited uracil and thymine, *J. Phys. Chem. A* 111 (2007) 8500–8508.
- [10] T. Mori, W. Glover, M. Schuurman, T. Martínez, Role of Rydberg States in the Photochemical Dynamics of Ethylene, *J. Phys. Chem. A* 116 (2012) 2808–2818.
- [11] G. Worth, M. Robb, I. Burghardt, A novel algorithm for non-adiabatic direct dynamics using variational Gaussian wavepackets, *Faraday Discuss.* 127 (2004) 307.
- [12] G. Richings, I. Polyak, K. Spinlove, G. Worth, I. Burghardt, B. Lasorne, Quantum dynamics simulations using Gaussian wavepackets: the vMCG method, *Int. Rev. Phys. Chem.* 34 (2015) 269–308.
- [13] B. Lasorne, F. Sicilia, M. J. Bearpark, M. A. Robb, G. A. Worth, L. Blancafort, Automatic generation of active coordinates for quantum dynamics calculations: Application to the dynamics of benzene photochem-

- istry, *J. Chem. Phys.* 128 (2008) 124307–124310.
- [14] B. Lasorne, M. J. Bearpark, M. A. Robb, G. A. Worth, Controlling S1/S0 Decay and the Balance between Photochemistry and Photostability in Benzene: A Direct Quantum Dynamics Study, *J. Phys. Chem. A* 112 (2008) 13017–13027.
- [15] B. Lasorne, M. A. Robb, G. A. Worth, Direct quantum dynamics using variational multi-configuration Gaussian wavepackets. Implementation details and test case., *PCCP* 9 (2007) 3210 – 3227.
- [16] D. Mendive-Tapia, B. Lasorne, G. Worth, M. Bearpark, M. Robb, Controlling the mechanism of fulvene S1/S0 decay: switching off the stepwise population transfer, *Phys. Chem. Chem. Phys.* 12 (2010) 15725–15733.
- [17] D. Mendive-Tapia, B. Lasorne, G. Worth, M. Robb, M. Bearpark, Towards converging non-adiabatic direct dynamics calculations using frozen-width variational Gaussian product basis functions, *J. Chem. Phys.* 137 (2012) 22A548/1–10.
- [18] C. Allan, B. Lasorne, G. Worth, M. Robb, A Straightforward Method of Analysis for Direct Quantum Dynamics: Application to the Photochemistry of a Model Cyanine, *J. Phys. Chem. A* 114 (2010) 8713–8729.
- [19] D. Asturiol, B. Lasorne, G. Worth, M. Bearpark, M. Robb, Exploring the sloped-to-peaked S2/S1 seam of intersection of thymine with electronic structure and direct quantum dynamics calculations, *Phys. Chem. Chem. Phys.* 12 (2010) 4949–4958.
- [20] M. Araújo, B. Lasorne, A. Magalhaes, M. Bearpark, M. Robb, Controlling Product Selection in the Photodissociation of Formaldehyde: Direct Quantum Dynamics from the S1 Barrier, *J. Phys. Chem. A* 114 (2010) 12016–12020.
- [21] A. Thiel, H. Köppel, Proposal and numerical test of a simple diabaticization scheme, *J. Chem. Phys.* 110 (1999) 9371–9383.
- [22] H. Köppel, J. Gronki, S. Mahapatra, Construction scheme for regularized diabatic states, *J. Chem. Phys.* 115 (2001) 2377–2388.
- [23] H. Köppel, B. Schubert, The concept of regularized diabatic states for a general conical intersection, *Mol. Phys.* 104 (2006) 1069–1079.
- [24] G. Richings, G. Worth, A Practical Diabatisation Scheme for Use with the Direct-Dynamics Variational Multi-Configuration Gaussian Method, *J. Phys. Chem. A* 119 (2015) 12457–12470.
- [25] G. Worth, P. Hunt, M. Robb, Non-adiabatic dynamics: A comparison of surface hopping direct dynamics with quantum wavepacket calculations, *J. Phys. Chem. A* 107 (2003) 621–631.
- [26] D. Asturiol, B. Lasorne, M. Robb, L. Blancafort, Photophysics of the π, π^* and n, π^* states of Thymine: MS-CASPT2 Minimum-Energy Paths and CASSCF on-the-Fly Dynamics, *J. Phys. Chem. A* 113 (2009) 10211–10218.
- [27] Z. Lan, E. Fabiano, W. Thiel, Photoinduced Nonadiabatic Dynamics of Pyrimidine Nucleobases: On-the-Fly Surface-

- Hopping Study with Semiempirical Methods, *J. Phys. Chem. B* 113 (2009) 3548–3555. 690
- [28] J. Szymczak, M. Barbatti, J. S. Hoo, J. Adkins, T. Windus, D. Nachtigallová, H. Lischka, Photodynamics Simulations of Thymine: Relaxation into the First Excited Singlet State, *J. Phys. Chem. A* 113 (2009) 12686–12693. 695
- [29] M. Merchán, R. González-Luque, T. Climent, L. Serrano-Andrés, E. Rodríguez, M. Reguero, D. Peláez, Unified Model for the Ultrafast Decay of Pyrimidine Nucleobases, *J. Phys. Chem. B* 110 (2006) 26471–26476. 700
- [30] B. West, J. Womick, A. Moran, Interplay between Vibrational Energy Transfer and Excited State Deactivation in DNA Components, *J. Phys. Chem. A* 117 (2013) 5865–5874. 705
- [31] Y. He, C. Wu, W. Kong, Photophysics of Methyl-Substituted Uracils and Thymines and Their Water Complexes in the Gas Phase, *J. Phys. Chem. A* 108 (2004) 943–949. 710
- [32] J. Peon, A. Zewail, DNA/RNA nucleotides and nucleosides: direct measurement of excited-state lifetimes by femtosecond fluorescence up-conversion, *Chem. Phys. Lett.* 348 (2001) 255–262. 715
- [33] R. Improta, F. Santoro, L. Blancafort, Quantum Mechanical Studies on the Photophysics and the Photochemistry of Nucleic Acids and Nucleobases, *Chem. Rev.* 116 (2016) 3540–3593. 720
- [34] C. Crespo-Hernández, B. Cohen, P. Hare, B. Kohler, Ultrafast excited-state dynamics in nucleic acids, *Chem. Rev.* 104 (2004) 1977–2019. 725
- [35] B. Kohler, Nonradiative Decay Mechanisms in DNA Model Systems, *J. Phys. Chem. Lett.* 1 (2010) 2047–2053.
- [36] G. Richings, I. Polyak, K. Spinlove, G. Worth, I. Burghardt, B. Lasorne, Quantum Dynamics Simulations using Gaussian Wavepacket: The vMCG Method, *Int. Rev. Phys. Chem.* 34 (2015) 269–308.
- [37] M. Baer, Adiabatic and diabatic representations for atom-molecule collisions: Treatment of the collinear arrangement, *Chem. Phys. Lett* 35 (1975) 112–118. 730
- [38] N. Matsunaga, D. R. Yarkony, Energies and derivative couplings in the vicinity of a conical intersection 3. the 'most' diabatic basis, *Mol. Phys.* 93 (1998) 79–84. 740
- [39] B. Esry, H. Sadeghpour, Split diabatic representation, *Phys. Rev. A* 68 (2003) 042706/1–8. 745
- [40] M. Baer, T. Ve'rtesi, G. Halasz, A. Vibok, S. Suhai, On diabatization and the topological D-matrix: Theory and numerical studies of the H + H₂ system and the C₂H₂ molecule, *Faraday Discuss.* 127 (2004) 337–353. 750
- [41] D. R. Yarkony, On the consequences of non-removable derivative couplings. I. The geometric phase and quasidiabatic states. A numerical study, *J. Chem. Phys.* 105 (1996) 10456–10461. 755
- [42] H.-J. Werner, P. J. Knowles, G. Knizia, F. R. Manby, M. Schütz, and others, Molpro, version 2015.1, Tech. rep., www.molpro.net (2015). 760

- [43] G. A. Worth, K. Giri, G. Richings, I. Burghardt, M. H. Beck, A. Jäckle, H.-D. Meyer, The QUANTICS Package, Version 1.1, Tech. rep., University of Birmingham, Birmingham, UK (2016).